Polymer Diffusion in Semicrystalline Polymers. 1. Poly(ether imide)/Poly(aryl ether ketone ketone)

Steven R. Lustig,† John G. Van Alsten,*,† and Benjamin Hsiao‡

Central Science Division and Fibers Research Division, DuPont Company, Experimental Station, Route 141, Wilmington, Delaware 19880-0356

Received February 19, 1993; Revised Manuscript Received May 3, 1993

ABSTRACT: The transport of poly(ether imide) (PEI) into amorphous and semicrystalline matrices of poly(aryl ether ketone ketone) (PEKK) has been characterized quantitiatively. Diffusion measurements were performed by an infrared attenuated total reflectance technique and the semicrystalline morphology investigated both before and after transport via DSC, TEM, SEM, WAXS, SAXS, and microtomy/FTIR. Fickian interdiffusion occurs when these polymers are in contact as melts. Two distinct time scales of sorption kinetics are observed during PEI transport into PEKK with a stable semicrystalline morphology. The early time transport is Fickian mutual diffusion although the amount of PEI imbibed remains far below that expected for complete miscibility in the PEKK amorphous phase. The mutual diffusivity activation energy increases from 9 kcal/mol in amorphous PEKK to 30 kcal/mol for the early time regime in semicrystalline PEKK. The suppression of the PEKK matrix mobility significantly hinders transport. The existence of slower transport in a later-time, kinetics regime is identified with a time scale over which macromolecules explore bottlenecks between crystalline obstacles. The competitive evolution of PEKK spherulites during mutual diffusion both significantly retards the transport kinetics and diminishes the total sorption of PEI.

Introduction

Polymer diffusion between a semicrystalline matrix and an amorphous bonding resin which results in sorption and entanglement is an interesting phenomenon. While great strides have been made in the understanding of the macromolecular diffusion in solutions, gels, and melts, very little information is available on the transport of macromolecules through semicrystalline materials. This is somewhat surprising considering the large number of high-performance engineering thermoplastics normally processed in this state. Transport in semicrystalline media can be influenced by factors such as the extent and distribution of crystallinity as well as the topology and swellability of the intercrystalline, amorphous fraction. Hence, these systems can exhibit intriguingly deviant behavior from amorphous systems.

Very few experimental studies of polymer transport in semicrystalline polymer systems have been reported to date. Diffusion in blends during crystallization and/or phase separation has been studied more extensively, e.g., refs 1–7. In these situations distinct morphologies are created depending on the relative mobilities of the components during phase separation. Tead *et al.*[8] used forward recoil spectroscopy to characterize the limited interdiffusion between poly(amic acid) and polyimide films. Although there exists segmental orientation is this system, transport is limited primarily by the glass transition. Filippov *et al.*[9] characterized the time-dependent mobility of oligo(propylene oxide) in the intercrystalline regions of poly(ethylene oxide) using pulsed field gradient NMR. The observed oligomer mobility exhibits limiting, steady-state values in two time regimes: at early times as the oligomer is believed trapped within intercrystalline regions (high diffusivity plateau at ca. 10^{-15} cm^2/s) and at long times as the oligomers explore length scales much greater than the crystallites (low diffusivity plateau at ca. 10^{-16} cm^2/s). Mechanical properties of thermoplastic interlayer bonds between semicrystalline composite polymers have been reported by Meakin *et al.*[10] As far as we are aware, quantitative characterizations of transport kinetics and morphology have not been previously reported for macromolecular transport into a semicrystalline polymer matrix.

The few available theories and simulations of macromolecular diffusion in porous media probably provide only a very limited foundation for understanding polymer diffusion in semicrystalline polymers since semicrystalline media are considerably more complex. The Fick–Jacobs equation describes diffusion through pore cross-sectional constrictions and expansions, although the behavior is well characterized only at long times when an effective diffusivity can be defined.[11] Teraoka *et al.*[12] describe reptation of polymers whose persistence length is greater than the pore radius of a surrounding porous medium. Aspects of macromolecular transport in disordered and porous media have been treated using effective medium theory (EMT), e.g., refs 13–15. Since EMT is very sensitive to the assumed interphase connectivity,[15] its application fails to predict even small-molecule transport in blends when the theoretical and experimental morphological topologies are not well matched.[16] Alternatively, computer models have simulated macromolecular dynamics and transport in porous and random media.[17-19] In media with porosities greater than the critical percolation threshold, the center-of-mass mean-square displacement, $\langle R^2(t)\rangle$, is predicted to be Fickian, i.e., proportional to time, t, at early times (Rouse-like diffusion within a pore) and at long times (diffusion well beyond a pore branch length). Non-Fickian transport is expected at intermediate times when displacements and topological constraints are of comparable length scales. In semicrystalline polymeric media, a wide distribution of effective topological constraints are possible. Depending on the relative length scales of the diffusing chain dimension and the crystallite topological constraints, macromolecular transport could exhibit deviations from Fickian kinetics during experimentally relevant time scales.

In this work we study the transport of an amorphous poly(ether imide) (PEI) into typical high-performance,

† Central Science Division.
‡ Fibers Research Division.

0024-9297/93/2226-3885$04.00/0

semicrystalline matrices, namely, poly(aryl ether ketone ketone) (PEKK) copolymers. PEKKs are particularly interesting copolymers in which the semicrystalline spherulite morphologies are readily controlled by annealing. Crystalline melting temperatures change with PEKK copolymer composition. Previous works have characterized PEKK crystallization temperatures, kinetics, and morphologies[20-24] as well as the properties of PEKK/PEI mixtures crystallized after blending.[24] PEI and PEKK copolymers form miscible blends at all compositions in their melts. PEKK is the only crystallizable component in the blend. In amorphous blends a single glass transition temperature changes with relative composition as described by the Fox equation. Higher transition temperature deviations, up to +30 °C, occur for semicrystalline blends. The Flory–Huggins interaction parameter (enthalpy of mixing) is negative although near zero.[24] Now we apply an infrared technique[25] recently developed in our laboratory to characterize quantitatively the transport kinetics. New morphological characterizations of the semicrystalline PEKK matrices are also provided before and after PEI imbibition.

Experimental Section

Materials and Preparation. Developmental grade PEKKs were prepared from diphenyl ether (DPE), terephthalic acid (T), and isophthalic acid (I) in a two-step process at DuPont. The PEKK polymers have the chemical structure shown below:[20]

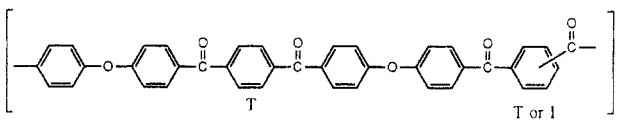

In this structure the diagonal line indicates that these materials are copolymers of terephthaloyl (para) and isophthaloyl (meta) ketone linkages. Because of the synthetic route, these polymers can be thought of as copolymers of diads -DPE-T-DPE-T- (TT) and/or -DPE-T-DPE-I- (TI). In all cases the isophthalate units are separated by a minimum of five phenyl groups.[5] In this study, we utilized PEKKs of three different terephthaloyl to isophthaloyl (T/I) ratio compositions, PEKK (70/30), PEKK (60/40), and PEKK (15/85). All three materials have weight-average molecular weights (M_w) of about 1×10^5 amu and number-average molecular weights (M_n) of about 3×10^4 amu. The equilibrium melting temperatures are near 355, 330, and 270 °C, respectively, and glass transition temperatures are of ca. 155 °C. The variance of the terephthaloyl to isophthaloyl (T/I) ratio results in marked changes in both thermal and dielectric properties.[21]

PEKK films of thicknes 125 μm were first melt quenched. These films were subsequently crystallized by annealing between sheets of Kapton 500HN film in the preheated platens of a hydraulic press. Scanning electron micrographs indicate these films are smooth to length scales smaller than 0.01 μm. The films were characterized both before and after diffusion experiments via differential scanning calorimetry (DSC), wide-angle X-ray scattering (WAXS), and small-angle X-ray scattering (SAXS) measurements as described below. PEKK matrices are designated in the following text according to the temperature and duration of their annealing treatments.

The chosen PEI material was General Electric's Ultem 1000, which has the chemical repeat unit:

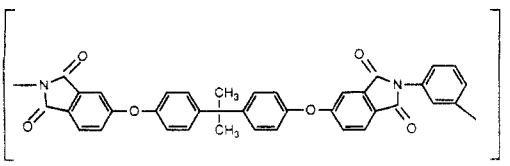

This material is noncrystallizable and has a T_g of about 216 °C and a weight-average molecular weight of approximately 3.5×10^4 amu. PEI was obtained in the form of pellets which were dissolved in methylene chloride or chloroform to give 5 wt % concentration of polymer in solvent. These solutions were used to produce thin films via spin coating directly onto the optical elements used in our diffusion experiments.

X-ray Scattering Characterizations. The weight fraction degree of crystallinity was inferred by WAXS using an automated Philips diffractometer and Cu Kα radiation. Data were collected in a fixed time mode with a step size of 0.05° 2θ and run from 4° to 65° 2θ. The diffraction pattern from a noncrystalline sample of the same composition was scaled and subtracted from the semicrystalline pattern. The degree of crystallinity was defined as the ratio of the area under the residual crystalline pattern divided by the total scattering in the original pattern. The crystal volume fraction, x_C, was inferred from the degree of crystallinity and the densities of the amorphous and crystalline phases, 1.278 and 1.402 g/cm^3, respectively.

SAXS was carried out with Kratky optics using a scintillation counter of Ni-filtered Cu Kα radiation. The data were collected in a step size of 0.01° 2θ and run from 0.12° to 1.4° 2θ. Data were subsequently desmeared and Lorenz-corrected. No standards were run to calibrate the absolute intensity. The scattering data were corrected for thermal density fluctuations using Porod's law.

$$I(q) = I_b + A_p/q^4 \tag{1}$$

where I_b represents the electron density fluctuation and A_p is Porod's asymptote. In addition, the scattering density was corrected for the diffuse boundary thickness between the crystalline and amorphous regions.[26] The correlation function $\gamma(r)$ was calculated by the Fourier transform of the scattering intensity.

$$\gamma(r) = \frac{1}{2\pi^2}\int_0^\infty \tilde{I}(q)\, q^2 \cos(qr)\, dq \tag{2}$$

where the corrected intensity, $\tilde{I}(q)$, was extrapolated in the limits near zero and at large q using the Porod equation.

A method of using the SAXS correlation function to estimate lamellar geometry in semicrystalline systems is discussed in detail elsewhere.[27-30] Two lamellar variables were estimated from the correlation function. The value of the lamellar bundle long period, L, was determined from the position of the first maximum. The linear degree of crystallinity, x_{CL}, within the lamellar bundles was determined from a two-phase model

$$B = x_{CL}(1-x_{CL})L \tag{3}$$

where B is the first intercept with the $\gamma(r) = 0$ line.

Diffusion Measurements. Diffusion experiments were performed using the infrared attenuated total reflectance (ATR-FTIR) technique described in a previous publication.[25] A film ca. 0.5 μm thick of PEI is adhered onto a silicon ATR element via spin coating from solution. A PEKK matrix ca. 120 μm thick is subsequently placed on the PEI. The layers are fixed inside a high-temperature ATR assembly of an FTIR spectrometer. Isothermal diffusion measurements were monitored *in situ* at temperatures ranging from 240 to 310 °C with the temperature controlled to within 2 °C. The dissolution of the PEI into the PEKK matrix was tracked by measuring as a function of time the Bisphenol A methyl group C–H stretch absorbance, A_t, at 2969 cm^{-1}. We believe spin coating provides essentially complete interfacial contact between the ATR crystal and the PEI spin-coat film. During the onset of interlayer transport, the high interfacial smoothness between the PEI/PEKK layers permits relatively fast molecular contact as the system is heated above the PEI glass transition temperature.

These infrared absorbance data can be subsequently fit to an appropriate model to yield the coefficient of mutual diffusion. The mathematical formulations of two useful models are described in the appendix. For Fickian diffusion between two miscible, stratified phases, the dimensionless sorption is a function

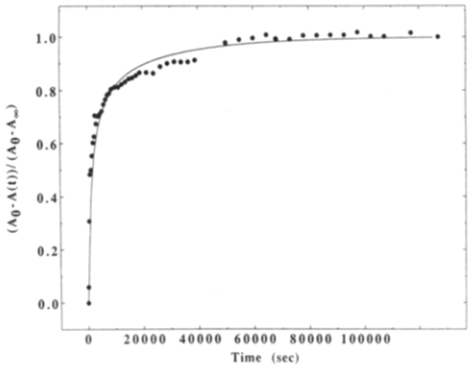

Figure 1. Dimensionless infrared absorbance data for the mutual diffusion between PEI and PEKK (15/85) melts at 280 °C (circles) and the best fit of eq 4 (solid curve).

of time, t, as described below:[25]

$$\frac{A_t - A_0}{A_\infty - A_0} = 1 - \frac{\frac{2}{\pi}\sum_{n=1}^{\infty} \frac{\sin\left(n\pi\frac{b}{a}\right)}{n} \exp\left(-n^2\pi^2\frac{Dt}{a^2}\right)\left[\frac{1+(-1)^{n+1}\exp\left(\frac{-2a}{\lambda}\right)}{1+\left(\frac{n\pi\lambda}{2a}\right)^2}\right]}{\left[1-\exp\left(\frac{-2b}{\lambda}\right)\right] - \frac{b}{a}\left[1-\exp\left(\frac{-2a}{\lambda}\right)\right]} \quad (4)$$

In this expression A_0 and A_∞ are the initial and long-time infrared absorbances, a is the initial total polymer system thickness on the ATR element, b is the initial thickness of the PEI coating, λ is the infrared evanescent penetration depth,[31] and D is the mutual diffusion coefficient. A value for λ of ca. 0.26 μm at an incident angle of 45° is determined independently from the diffusion data using the refractive indices of the silicon ATR element[32] and PEKK. The refractive index of PEKK at 2969 cm^{-1} was inferred by fitting the angular dependence of the reflectivity of a crystallized PEKK sample to Fresnel's equation as described elsewhere.[25] The spin-coat layer thickness is measured via spectroscopic ellipsometry. Depth profiling was performed using an infrared microscope to analyze microtomed samples of some systems. PEKK/PEI diffusion couples were first embedded in epoxy and then sliced to a thickness of 900 nm.

Transmission Electron Microscopy. Permanganate etching was performed for transmission electron microscopy. The etching solution and preparation technique for PEKK has been described previously.[23] Etched samples were then exposed to a carbon–platinum vapor at low angle inside a vacuum evaporator, coated with poly(acrylic acid) solution, and dried. The dry replica was stripped and was vacuum evaporated with carbon. The poly(acrylic acid) coating was then dissolved in water, and the remaining replica was picked up on copper mesh grids, dried, and transferred to the microscope. The electron microscopy was performed on a JEOL 200FX transmission instrument. Images were obtained at 100-kV accelerating voltage and recorded on film.

Results

PEI Diffusion in Amorphous PEKK. First, we illustrate the simplest transport problem, which is diffusion of PEI in a completely molten matrix of PEKK (15/85). An ATR-FTIR diffusion experiment was performed at 280 °C, approximately 10 °C above the equilibrium melting temperature of this matrix polymer. The time-dependent, PEI infrared absorbance during sorption in the PEKK melt is illustrated in Figure 1. It is also demonstrated that the Fickian model in eq 4 describes well the infrared absorbance sorption data. We calculate a diffusion coefficient of 9.1 (±1.5) × 10^{-12} cm^2/s. While uncertainties in the values of λ, a, and b contribute to the uncertainty in the diffusivity, the greatest source of uncertainty from this data set is the scatter of data about the diffusion model due to the integrations of absorption peaks. A valid fit of the model to these data implies that the PEI and PEKK interdiffuse and are mutually soluble as amorphous polymers.

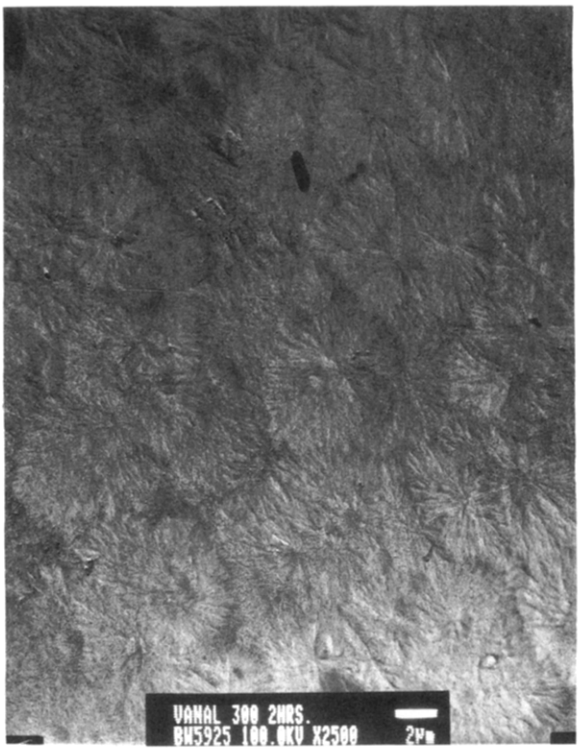

Figure 2. TEM of a PEKK (70/30) sample which has been annealed for 3 h at 250 °C, etched, and replicated at the matrix surface. Note the complete impingement of spherulites.

It is also of interest to compare the diffusivity activation energy of PEI in PEKK relative to the self-diffusivities of polyethylene and polystyrene melts. The PEI/PEKK (15/85) diffusion experiment was repeated at 240 °C to estimate an activation energy for the PEI diffusivity. An Arrhenius plot indicates an activation energy of 9 kcal/mol. Since these diffusion experiments occur at relatively high temperatures, we compare the relative activation and thermal energy ratio, E_a/RT, for a PEI/PEKK mutual diffusion of ca. 18 relative to characteristic values of 6 and 20 for self-diffusion in polyethylene and polystyrene, respectively, at 175 °C.[33] Hence, in our experiments the average PEI/PEKK dynamic stiffness which depends on the barriers to chain backbone rotation is as comparable to the chain's kinetic energy as the corresponding barriers in other thermoplastic melts.

PEI Transport in Semicrystalline PEKK. PEI transport is considerably more hindered in semicrystalline PEKK. A PEKK (70/30) matrix was annealed at 250 °C for 3 h. At this temperature the annealing time is several orders of magnitude greater than the crystallization half-time.[22] The TEM photograph at the matrix surface in Figure 2 illustrates the spherulites grow to complete domain impingement. Figure 3 illustrates a polarized optical micrograph of an identical PEKK (70/30) sample microtomed in the plane transverse to the direction of diffusion. It is apparent that spherulites are randomly nucleated without obvious bias near the surface and in the bulk. The volume degree of crystallinity measured for this system inferred from WAXS is ca. 30% (see Table I). The time-dependent infrared PEI absorbance during

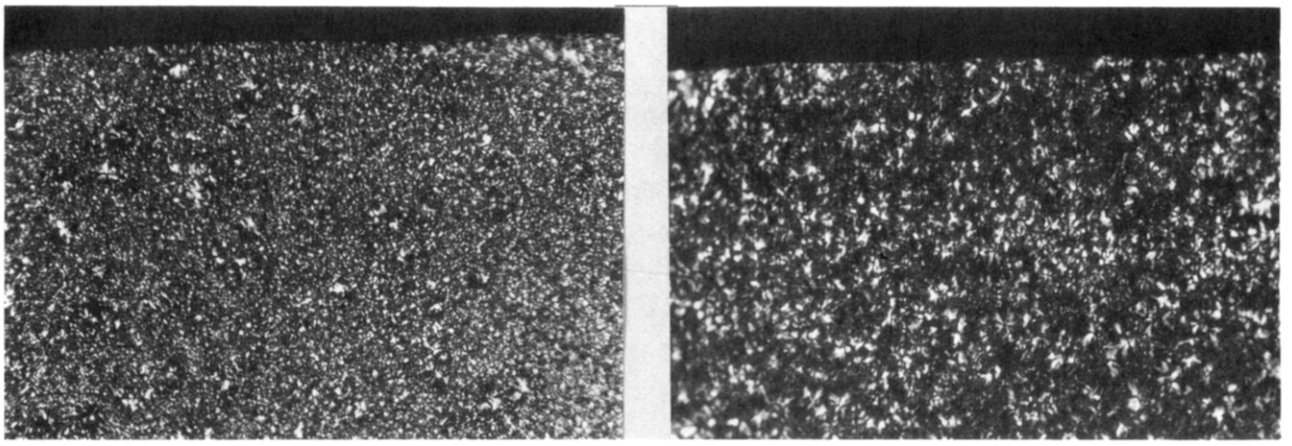

Figure 3. Polarized optical micrograph of a PEKK (70/30) matrix annealed for 3 h at 250 °C and microtomed in the plane transverse to the direction of diffusion. Bright spots indicate spherulite nuclei. The film is magnified at 410× (left) and at 650× (right) where the surface (top) would be in contact with PEI.

Table I. PEKK (70/30) Matrix Characteristic Parameters: SAXS Long Period, L; SAXS Linear Degree of Crystallinity, x_{CL}; SAXS Lamellar Thickness, l_C; SAXS Interlamellar Amorphous Gap, l_A; WAXS Volume Degree of Crystallinity, x_C[a]

matrix annealing conditions						
temp (°C)	time (h)	L (Å)	x_{CL} (v/v %)	l_C (Å)	l_A (Å)	x_C (v/v %)
250	3*	128	71	91	37	30
	3†	122	73	89	33	28
205	2*	102	72	73	29	32
300	2*	153	74	113	40	28

[a] Characterizations are performed either before (*) or after (†) PEI sorption.

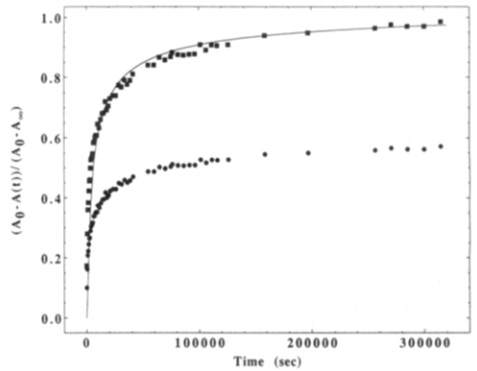

Figure 4. Dimensionless sorption of PEI at 280 °C into semicrystalline PEKK (70/30) previously annealed for 3 h at 250 °C. The data are normalized assuming total PEI miscibility (circles) and the absorbance at the early time regime plateau (squares). The best fit of eq 4 to the latter data (line) yields an effective diffusion coefficient of 7×10^{-13} cm^2/s.

sorption in the PEKK matrix at 280 °C is illustrated in Figure 4. In the bottom curve the infrared absorbance sorption data are normalized by the hypothetical, infinite-time absorbance corresponding to complete and uniform PEI dissolution in the PEKK matrix. PEI transport is relatively rapid at early times, although at long times an apparent sorption plateau is observed. We observe that transport continues, however, at much slower rates as illustrated when the data are plotted on a logarithmic time scale in Figure 5. The apparent plateau noted on a linear time scale occurs at the change in slope on the logarithmic time axis. We shall distinguish between these early and later time regimes of the sorption kinetics in a subsequent discussion. At the onset of the apparent plateau the total amount of PEI imbibed into the PEKK at ca. 55% is considerably diminished relative to its expected miscibility

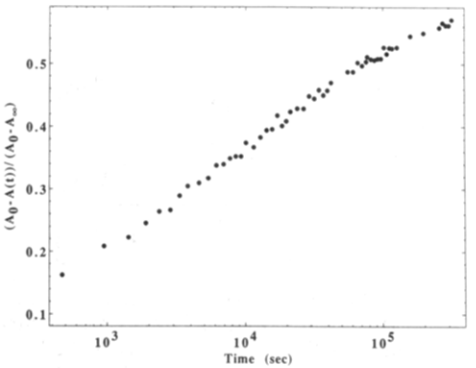

Figure 5. Dimensionless sorption of PEI at 280 °C into semicrystalline PEKK (70/30) previously annealed for 3 h at 250 °C. The data are normalized assuming total PEI miscibility and shown with logarithmic time scale abscissa.

in the amorphous phase. The maximum penetration of the PEI into the PEKK (70/30) can be estimated from the "best-case", amorphous-phase diffusion coefficient of the PEKK (15/85) system. After 3×10^5 s the PEI root-mean-squared penetration would be approximately 23 μm (estimated via the characteristic random-walk distance $(2Dt)^{1/2}$) only one-fifth the total thickness of the PEKK matrix. Therefore, the apparent plateau in the sorption clearly is not representative of complete PEI saturation in the semicrystalline PEKK matrix. Instead, it is evident that the PEI macromolecules have penetrated through only a fraction of the matrix thickness during the early time regime.

To estimate the depth of PEI penetration, we have performed infrared measurements on the PEKK (70/30) matrix material recovered post diffusion by microtoming in the plane of the film. The presence of PEI in the PEKK is indicated by the PEI carbonyl absorbance band at 1724 cm^{-1}. We succeeded in sampling to a depth of ca. 11 μm and confirmed the presence of PEI to at least this depth. Since this depth is on the order of ca. 5 diameters of impinging PEKK (70/30) spherullites, we believe that it is well beyond the thickness to be expected of an amorphous skin. The PEI carbonyl absorbance at 1724 cm^{-1} can be compared to the PEKK carbonyl peak at 1658 cm^{-1} to estimate an order of magnitude concentration of PEI imbibed, assuming that the carbonyl oscillator strengths of these two vibrations are equivalent. We estimate PEI concentrations of 2 ± 1% through the penetrated depth given the uncertainties in evaluating peak heights and the approximation of equivalent oscillator strength. From this estimate it is also possible to calculate

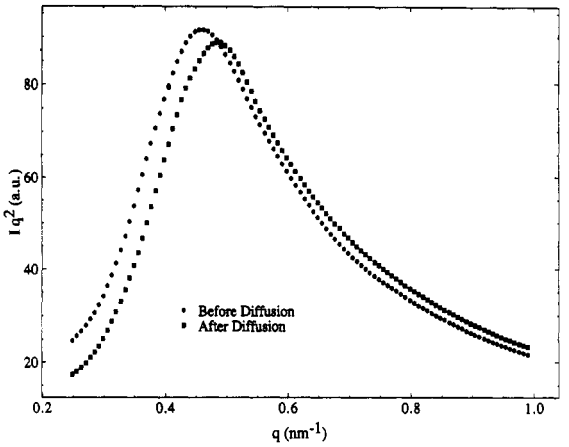

Figure 6. Lorenz-corrected SAXS intensity as a function of wave vector from the sample of the PEKK (70/30) matrix in Figure 4 before (circles) and after (squares) PEI imbibition at 280 °C.

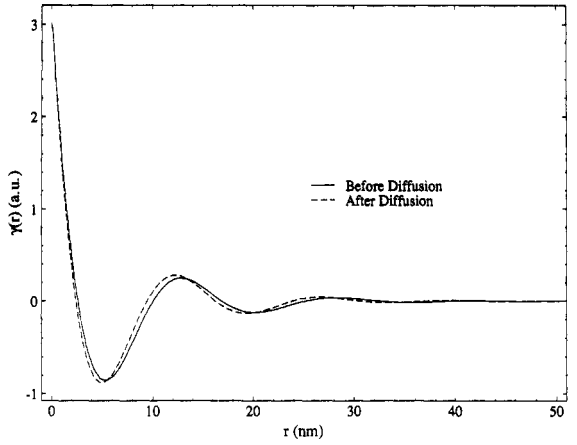

Figure 7. Correlation functions obained from the data of Figure 6. This analysis provides the lamellar long period and the degree of crystallinity within the lamellar bundles summarized in Table I.

a penetration length for PEI by coupling the PEI mass balance to the experimentally determined values of the infrared absorbance at the beginning and end of the experiment. The analysis outlined in the appendix suggests a ca. 30-μm penetration length of PEI into PEKK (70/30).

Our experimental characterizations of the PEI/PEKK (70/30) system suggest that very little change in the spherulite morphology occurs during the sorption of PEI. SAXS and WAXS parameters before and after PEI sorption are summarized in Table I. The Lorenz-corrected SAXS intensities are plotted as a function of scattering vector in Figure 6. There is a slight shift in the position at the peak intensity from 0.45 to 0.47 nm^{-1} after PEI sorption. This implies either an increase in the electron density near crystal lamellae or a thickening of the lamellae themselves. There is also only a modest decrease in the SAXS peak intensity from 91 to 88 au. The apparent decrease in the total degree of crystallinity results most likely from the dilution of crystallites by the amorphous PEI. We regard this apparent change with some discretion, however, since the absolute intensities are not calibrated. Figure 7 illustrates the counterpart correlation functions to the SAXS data in Figure 6. The lamellar long period changes negligibly with a slight decrease in the degree of crystallinity from 71 to 73 v/v %. WAXS estimates of the total volume crystallinity decrease comparably from 30 to 28 v/v %. Differential scanning calorigrams illustrated in Figure 8 are essentially identical. There is only slight

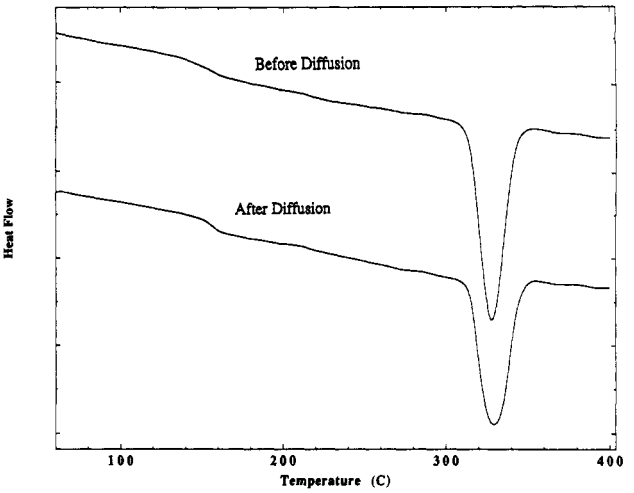

Figure 8. DSC scans for PEKK (70/30) annealed for 2 h at 250 °C (upper) and after PEI imbibition at 280 °C for 3×10^5 s (lower).

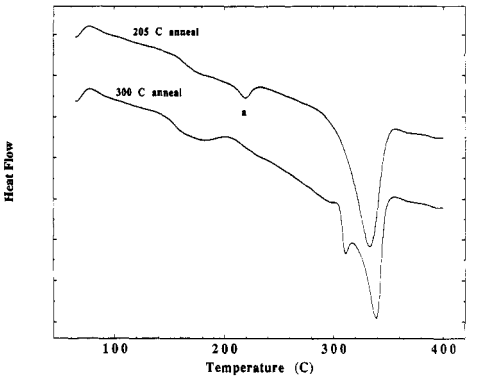

Figure 9. DSC scans for PEKK (70/30) crystallized for 2 h at 205 °C (upper curve) where peak "a" is due to the melting of small crystallites within the spherulites. An identical sample crystallized at 300 °C (lower curve) implies a different morphology is formed due to a higher melting subpopulation of crystallites.

evidence for the amplification of the environments associated with the lower melting tail. Changes in the PEKK (70/30) during PEI imbibition are minute and consistent with simple dilution or a slight interfacial broadening of lamellae in contact with PEI. Hence, we believe the overall semicrystalline morphology is reasonably constant throughout this diffusion experiment.

We now illustrate the influence of the PEKK semicrystalline morphology on PEI transport. Although PEKK can be crystallized at approximately the same rate by annealing at temperatures near the glass transition and melting point limits, the spherulite sizes and morphologies produced are markedly different. The upper and lower curves of Figure 9 illustrate the DSC scans of two samples of PEKK (70/30) annealed for 2 h at 205 and 300 °C. Both annealing times are slightly greater than the crystallization half-times at their respective temperatures.[22] The low-temperature treatment produces a distribution of lower melting, small crystallites (DSC peak "a") within the spherulites which restrict the amorphous phase and result in a higher T_g of 164 °C than the 155 °C T_g created by annealing at 300 °C. SAXS correlation functions in Figure 10 also illustrate the differences between these morphologies. Table I summarizes the SAXS and WAXS characterizations for these PEKK matrices. We note the total degrees of crystallinity which result from these two annealing conditions are comparable although the long period and interlamellar spacings are considerably larger for the 2-h annealing at 300 °C.

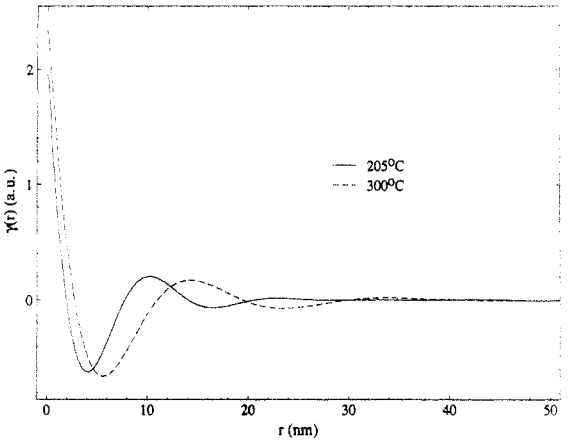

Figure 10. SAXS correlation functions for PEKK (70/30) samples in Figure 9 crystallized for 2 h at 205 °C (solid curve) and 300 °C (dashed curve). The lower melting crystallite subpopulation reduces the average scattering unit cell and interlamellar spacings.

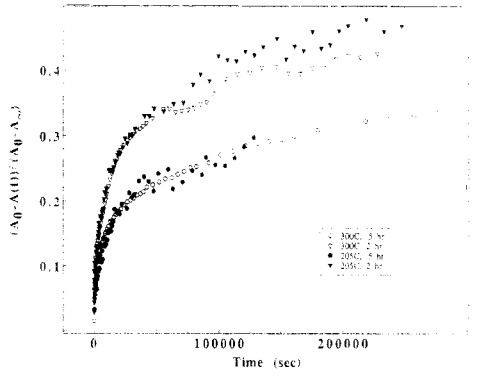

Figure 11. Dimensionless sorption of PEI into PEKK (70/30) at 280 °C. The PEKK samples were precrystallized for 2 h at 205 °C (solid triangle) and 300 °C (open triangle), as well as partially annealed for a half hour at 205 °C (solid circle) and 300 °C (open circle).

Several aspects of the semicrystalline morphology can limit polymer sorption in the early-time regime. Figure 11 presents the PEI sorption in PEKK (70/30) matrices which have been fully crystallized after annealing for 2 h at 205 and 300 °C. Despite the aforementioned differences in lamellar morphologies, the early-time PEI sorption rates are virtually identical. During the later-time sorption regime after ca. 5×10^4 s, the 300 °C annealing provides a greater hindrance to PEI imbibition. This hindrance corresponds to the larger SAXS long period. We might interpret this effect as the higher volume-filling lamellae providing more effective transport obstacles. Also included in Figure 11 are the sorption data in matrices which had been partially crystallized by annealing for 1 half hour at 205 and 300 °C. Although there is considerable scatter in the data, the early-time sorption rates are also sensibly identical, although slower than the early-time sorption rates in the more fully annealed matrices. The concomitant crystallization and rearrangement within the matrix does also hinder PEI sorption. These four sorption curves are directly comparable since their initial geometries and ATR penetration lengths are sensibly identical. Hence, we infer from the early-time sorption data of the static morphology that the details of crystalline size distribution are less important to the sorption kinetics than the total volume degree of crystallinity. The effect of simultaneous crystallization is explored further next.

PEI Transport with Concomitant PEKK Crystallization. In some welding applications macromolecular transport and interface formation occur during the competitive evolution of spherulite, semicrystalline morphologies. To study this competition, we first prepared amorphous films of PEKK (15/85), (60/40), and (70/30) via melt-quenching. The subsequent sorption kinetics of PEI in these matrices at 280 °C are illustrated in Figure 12. Gaps in the data collection occur during long experiments due to unfortuitous loss of liquid nitrogen from within the FTIR detector. However, the detector's original response is quickly reestablished upon refilling. Here the absorbance sorption curves are each normalized using their respective hypothetical, long-time absorbance assuming complete miscibility. PEKK (15/85) does not crystallize appreciably at this temperature, and full PEI mixing is attained. The data for the PEKK (60/40) and (70/30) clearly demonstrate competition between mutual diffusion and crystallization. Gardener *et al.*[23] have shown that PEKK crystallization kinetics increase with increasing the terephthaloyl comonomer content. Therefore, the total sorption of PEI scales inversely with the rate of matrix crystallization. Even the initial sorption rate is effectively retarded during matrix crystallization.

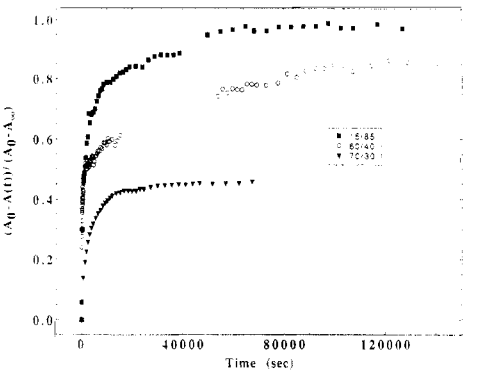

Figure 12. Dimensionless sorption of PEI at 280 °C into initially amorphous PEKKs of various copolymer (T/I) ratios.

Discussion

The aforementioned measurements of polymer transport kinetics indicate interesting sensitivities to the significant differences between amorphous and semicrystalline media. We now proceed to discuss the PEKK semicrystalline morphology and the mechanisms for the observed anomalous PEI sorption kinetics. First we will identify some of the salient features of the heterogeneities within the semicrystalline morphology. Next we will discuss some physical characteristics and two mathematical models to describe the transport phenomenology. Finally we will consider the importance of matrix relaxation during macromolecular transport in the early-time sorption kinetics.

Semicrystalline Morphology of PEKK. The semicrystalline PEKK materials form very common spherulite morphologies. Nucleation of the PEKK spherulites can be sufficiently concentrated to limit growth to an average size of ca. 6 μm before interdomain impingement. Figure 3 illustrates that the spherulite nucleation density is not sensibly biased near the film surface. In addition our SEM characterizations of PEKK materials also support the contention that any amorphous skin exists no deeper than 0.01 μm from the surface. The PEKK morphology is very similar to that of poly(aryl ether ketones) investigated elsewhere.[34] Crystalline lamellae are concentrated at the spherulite nucleus. Multilamellar dendrites originating from the spherulite nucleus branch sufficiently to maintain nearly parallel local alignment. The crystalline arrangement is heterogeneous. Even though spherulite impinge-

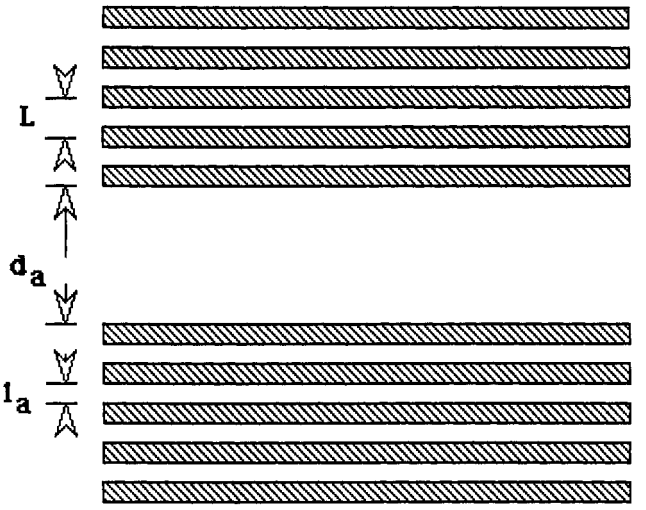

Figure 13. Schematic representation of a two-phase model showing bundles of five lamellae of long period L, separated by a large amorphous region of width d_a.

Table II. Estimates of the Average Thickness, d_A, and Volume Fraction, Φ_{pocket}, for the Amorphous Pocket between Lamellar Bundles of PEKK (70/30) Matrix Either before (*) or after (†) PEI Sorption

matrix annealing conditions			
temp (°C)	time (h)	d_A (Å)	Φ_{pocket} (v/v %)
250	3*	912	60
	3†	1013	64
205	2*	667	58
300	2*	1297	64

ment occurs, only a fraction of the total volume is occupied by the approximately regular lamellar stacking which gives a small-angle scattering maximum. This is consistent with the total degree of crystallinity, x_C, always being less than the linear crystallinity, x_{CL}, within the dendrites. Hence, there must be amorphous "pockets" present in between the spherulite domains and the lamellar bundles forming dendrites. In addition small crystallites can exist between dendrites emanating from the spherulite nucleus. It is expected that not all of the amorphous phase is equally accessible to a macromolecular diffusant.

The X-ray scattering measurements can be used to estimate how heterogeneously the amorphous phase is spatially distributed. These data were analyzed to estimate the lamellar long period L, linear crystallinity, x_{CL}, lamellar thickness, l_C, and amorphous layer thickness, l_A, which are summarized for several experiments in Table I. Since interspherulite impingement occurs, the amorphous phase occurs between dendrites. A simple, two-phase model can be constructed to estimate the average length scale of amorphous pockets, d_A, illustrated schematically in Figure 13. The quantities x_{CL} and x_C are related through a mass balance:

$$x_{CL}L = x_C\left(L + \frac{d_A - l_A}{n}\right) \tag{5}$$

where n is the number of lamellae within a bundle. If the sum of the lamellar bundle thickness and the distance between the lamellar bundles is small, <100 nm, then small-angle X-ray scattering arises from the density difference between the lamellar bundles. This implies that each coherently scattering lamellar bundle consists of between 3 and 6 lamellae.[29] Assuming there are 5 lamellar stems in the average bundle leads to estimates of amorphous pocket thicknesses presented in Table II. Clearly the quantitative values for this estimation are model dependent. Still, these order-of-magnitude length scale estimates are consistent with the average dendrite separations observed via microscopy.

Since segmental rearrangement between macromolecular species and matrix relaxation must occur during larger scale center-of-mass transport, transport occurs within the amorphous regions. It is apparent from Table II that a very large volume fraction of the crystallized matrix is comprised of large pockets of amorphous material regardless of crystallization conditions. Since crystalline domains are more concentrated within the spherulite near the point of nucleation, most of the macromolecular transport must occur through the spherulite periphery between dendrites and near boundaries between spherulite domains. The connectivity between these domains appears chaotic, although the spherulite structure creates more spatial correlation than is present in randomly percolated media. We will compare the transport phenomenologies between semicrystalline polymers and random media in the next section. We fully acknowledge that a two-phase model is too simple a picture for semicrystalline polymers. The current literature contains several experimental and theoretical arguments supporting the existence of a boundary, or interphase, between lamellar crystallites and amorphous regions. The existence of an interphase structure also hinders transport. The excess retardation of small-molecule transport due to the existence of crystallite interphases has been suggested much earlier.[37]

Transport in Semicrystalline PEKK. We now identify some of the physical aspects of the phenomenology associated with macromolecular transport in semicrystalline matrices. Not only does the typically low combinatorial entropy of mixing for polymer mixtures hinder miscibility,[35] but the heterogeneous semicrystalline morphology creates further entropic barriers to transport. Hence, transport is primarily motivated by an enthalpic driving force since the enthalpy of mixing is negative. The experimental characterizations imply spherulite nucleation is not biased near the PEKK surface and the imbibition of PEI into the PEKK occurs well beyond the characteristic skin depth. Hence, we believe the existence of the early-time sorption regime is not an interfacial effect.

We consider two mathematical diffusion models in order to interpret the sorption data in stable semicrystalline morphologies. The detailed model formulations are provided in the appendix. The continuous model assumes both polymer layers are completely miscible over all relevant concentrations during the experiment. This model has been discussed in detail previously[25] and results in the analytical solution provided in eq 4. We note this model contains only the mutual diffusivity as an adjustable parameter and does fit the mutual diffusion data between PEI/PEKK melts. This model does not describe the sorption of a PEI melt in a semicrystalline PEKK matrix since multiple time-scale sorption is observed. The second model considers the situation where the matrix can imbibe a penetrant only to a given concentration limit. Hence, a moving boundary exists at the edge of the matrix where the diffusant concentration attains its solubility concentration. There is no diffusive penetration of the matrix polymer into the diffusant as the matrix settles into the diffusant film. Both the diffusion coefficient and the solubility are adjustable parameters which are varied in attempts to fit this model to the experimental sorption data. However, we have been unable to fit the moving boundary model to any of the sorption data in semicrystalline PEKK with reasonable values of these adjustable parameters.

It is significant that the continuous model can provide a valid fit when the dimensionless infrared absorption sorption data are normalized by the experimentally determined values of the infrared absorbance at the early-time, apparent plateau. This modification requires the empirically-determined, apparent solubility. An example of this fit is illustrated in the top curve of Figure 4. The value of the effective diffusion coefficient 7.0 (±0.5) × 10^{-13} cm^2/s is over an order of magnitude lower than that obtained from the purely amorphous example. This modified model considers PEKK counterdiffusion which is also consistent with the observation that the PEKK infrared absorption bands increase simultaneously with the decrease in PEI absorption bands during transport. During the early-time regime, rapid PEI sorption occurs when PEI fills and exchanges with amorphous chains within the pockets between spherulite domains of PEKK. The amorphous domains which host this exchange are not necessarily limited to those with direct access to the PEI/PEKK interface. The low volume fraction of crystallites suggests the amorphous pockets percolate the matrix. However, the spherulites create a chaotic, although not perfectly random, percolated phase.

There are a few mechanisms which would result in the observation of distinct kinetic regimes during PEI sorption in semicrystalline PEKK. A spectrum of diffusivities would exist given polydispersity in the mixture. Although the PEI molecular weight distribution is polydisperse, we have recently observed the same phenomenology during the transport of highly monodisperse polystyrene in semicrystalline isotactic polystyrene matrices,[36] and work is continuing on this model system. Polydispersity in the size and tortuosity of the PEI pathways surely exists since the amorphous PEKK phase is distributed heterogeneously. The local PEI diffusivity would be considerably different between the constrained, interdendrite amorphous channels and the boundaries which define individual spherulite domains. In addition the existence of distinct kinetic regimes can be a signature of the chaotic, semicrystalline morphology itself.

Previous works have identified important signatures during transport in chaotic media. Sax and Ottino provide a brief review of modeling transport in composite media and further illustrate steady-state transport properties in media with entropic barriers.[38] The effective medium theory of Sahimi et al.[13] predicts only three kinds of behavior for transport in disordered media where only a fraction of the pathways transmit a random-walking diffusant. The analysis considers a single-bond effective medium approximation to the bond percolation threshold, p_c. The diffusant's mean-squared displacement remains localized for porosities below p_c, fractal with transport slower than Fickian for porosities near p_c, and classical Fickian diffusion for porosities above p_c. Ottino and Shah[39] have simulated transient sorption in these three percolation regimes which illustrate similar phenomenology. Classical sorption occurs for porosities above p_c. In media with porosities below p_c, there is pseudoclassical sorption to a diminished level of imbibition which depends on the total porosity. At this time no further sorption occurs, i.e., a second kinetic regime does not occur. The works of Muthukumar and Baumgartner[18] present simulations of Brownian chains between both randomly-distributed, impenetrable obstacles and regular entropic barriers. In random media there are three time regimes of transport behavior. At short times there are Fickian kinetics due to the unhindered displacement over distances smaller than the average separation between obstacles. At intermediate times the chain travels over length scales over which the pore space is fractal and anomalous diffusion kinetics result. The termination time which characterizes the crossover of the transport from anomalous to Fickian diffusion is greater than the configurational correlation time of the square radius of gyration. The intermediate anomalous diffusion has not been observed for periodically distributed obstacles although the motion of the chain between entropic barriers is retarded significantly by the bottlenecks connecting more open regions.

Only a limited reconciliation can be considered between the transport phenomenologies of PEI in semicrystalline PEKK and current knowledge of diffusion in media with random percolation. Hence, we approach this comparison with caution. The aforementioned works consider only entropic driving forces on systems in which there is no countercurrent transport. In addition, the available theories based on disordered, lattice-based composites illustrate a strong inadequacy for predicting the behavior of blends whose components are not topologically equivalent and the effective diffusivity is strongly dependent on morphology.[16] The arrangement of dendritic transport barriers creates correlated connectivity between polydisperse, amorphous pockets. Still the existence of multiple time-scale sorption kinetics is identifiable with the distinguishable length scales of chains in a random morphology. The critical threshold for a random percolation of a simple three-dimensional hexagonal lattice is 0.31 permeable volume fraction.[40] Table II shows that the total volume fraction of material found in the amorphous pockets ranges from 0.5 to 0.65. This suggests that the entire thickness of the matrix should be readily accessible to PEI macromolecules. Hence, the onset of the sub-Fickian sorption regime might not be identified as a signature of transport near the critical percolation threshold but instead a time scale over which the chains explore the bottlenecks between crystalline dendrites. The early-time regime mutual diffusion corresponds to displacements less hindered by interactions with the interfacial regions about crystalline lamellae. Hence, we infer that the two sorption time scales occur from the heterogeneously restricted pathways exchangeable between PEI and PEKK.

Matrix Relaxation during the Early-Time Regime. It is informative to compare the PEKK/PEI mutual diffusivity activation energies between the melt matrix and the early-time regime of the semicrystalline medium at comparable temperatures. We recognize the latter originates from effective diffusivities averaged over a heterogeneous medium. The continuous Fickian model was fit to the renormalized early-time PEI sorption data in PEKK (70/30) at 250, 280, and 310 °C. An activation energy of 30 kcal/mol is obtained from an Arrhenius plot. Notice this activation energy is over 3 times greater than the value obtained in the amorphous PEKK (15/85) melt. This implies that PEKK chains within the amorphous regions have a reduced ability to accommodate and rearrange with the diffusant macromolecules. Given the relatively low degree of polymerization for the PEI, we would also expect constraint release (tube renewal) to be an important mechanism during reptation in either the melt or interlamellar regions of a semicrystalline matrix. Hence, even the amorphous segments within the semicrystalline matrix could be sufficiently strained on the average to limit matrix relaxation and impede the chains' skeletal dynamics which mediate macromolecular transport.

Conclusions

This work provides some progress in the understanding of the bonding of a typical, high-performance thermoplastic with an amorphous polymer resin. Specifically, the penetration of PEI into matrices of a compatible semicrystalline PEKK has been explored. Two distinct time scales of sorption kinetics are observed during PEI transport into PEKK with a stable semicrystalline morphology. The early-time transport kinetics are Fickian although the amount imbibed remains far below that expected for complete miscibility in the amorphous phase. We infer that the two sorption time scales occur from the heterogeneously restricted pathways through which mobile PEI and PEKK interdiffuse. The occurrence of concomitant crystallization competes strongly with the rate and amount of PEI imbibed. Hence, there are interesting sensitivities of the transport phenomonology to the significant differences between amorphous and semicrystalline media. In subsequent papers we shall illustrate polymer transport in semicrystalline polymers using model systems.

Acknowledgment. We gratefully acknowledge the assistance of many skilled individuals (and their expertise): Brian Cox (ATR FTIR), Bill Kampert (DSC), Frank Wilson (SAXS), JoEllen Freida (WAXS), and Barbara Wood (TEM).

Appendix

Penetration Depth Estimation. It is possible to estimate the depth to which the PEI has penetrated the PEKK by applying a simple two-layer model of the diffusion couple. In this model, the following simplifications are applied: (1) The interface between the amorphous penetrant film and the semicrystalline film remains perfectly sharp. (2) Mass loss in the amorphous film is compensated by swelling of the semicrystalline phase so that the interfacial boundary moves toward the ATR element. (3) The swelling of the semicrystalline phase is uniform from the amorphous/semicrystalline interface to a characteristic penetration depth, beyond which the volume fraction of penetrant is zero. The infrared absorbance may be expressed as the sum of the integrated concentration profile weighted by the ATR evanescent detection field.

$$A_t = \int_0^{d_1} N_0 S \exp\left(\frac{-2z}{\lambda}\right) dz + \int_{d_1}^{d_2} N_1 S \exp\left(\frac{-2z}{\lambda}\right) dz \qquad \text{(A-1)}$$

In this expression, N_0 is the concentration of the PEI in the thin film, N_1 is the concentration of PEI in the PEKK, and λ is the depth of penetration of the infrared electric field. At $t = 0$, the absorbance for an oscillator characteristic of the penetrant is therefore

$$A_0 = \frac{\lambda N_0 S}{2}\left[1 - \exp\left(\frac{-2d_0}{\lambda}\right)\right] \qquad \text{(A-2)}$$

It is now possible to couple the solution of eq A-1,

$$A_t = \frac{\lambda N_0 S}{2}\left[1 - \exp\left(\frac{-2d_1}{\lambda}\right)\right] + \frac{\lambda N_1 S}{2}\left[\exp\left(\frac{-2d_1}{\lambda}\right) - \exp\left(\frac{-2d_2}{\lambda}\right)\right] \qquad \text{(A-3)}$$

with a mass balance

$$N_1(d_2 - d_1) = N_0(d_0 - d_1) \qquad \text{(A-4)}$$

and then divide by expression (A-2) to obtain the following result:

$$\frac{A_t}{A_0} = \frac{1 - \exp\left(\frac{-2d_1}{\lambda}\right)}{1 - \exp\left(\frac{-2d_0}{\lambda}\right)} + \frac{N_1}{N_0}\left\{\frac{\exp\left(\frac{-2d_1}{\lambda}\right) - \exp\left(\frac{-2}{\lambda}\left[d_0\frac{N_0}{N_1} + d_1\left\{1 - \frac{N_0}{N_1}\right\}\right]\right)}{1 - \exp\left(\frac{-2d_0}{\lambda}\right)}\right\} \qquad \text{(A-5)}$$

With the experimentally determined values of $A_{plateau}$, A_0, and d_0, and by estimating N_0/N_1 using data from the microtomy analysis, expression (A-5) may be solved iteratively to yield d_1 and thereby d_2, the thickness of the thin PEI film and the depth to which the PEI has permeated the PEKK, respectively.

Continuous and Moving Boundary Diffusion Models. Two types of models are considered to describe the mixing between the PEI and PEKK films via Fickian mutual diffusion. These models result in distinguishable mixing rates in terms of the time-dependent infrared absorbance bands which are measured experimentally. Here we describe only the formal specification of each model under consideration. We consider PEI to be the diffusant in a PEKK matrix.

The continuous model assumes both phases are completely miscible over all concentrations relevant during the experiment and has been discussed in detail previously.[25] Briefly, we consider diffusion of the thin film of diffusant with thickness b cast on the ATR element. Mutual diffusion occurs between the bounds of the element and the free surface of the matrix system. Since we expect undetectable changes in volume on mixing, the total thickness, a, of the polymer system remains constant.

$$\frac{\partial C}{\partial t} = D\frac{\partial^2 C}{\partial x^2} \qquad x \in [0,a], \quad \tau \in [0,\infty) \qquad \text{(A-6)}$$

Here $C{=}C(x,t)$ is the concentration of the polymer diffusant, x is position, and t is time, and we assume a constant diffusion coefficient, D. Since there can be no material flux across the boundaries, we require homogeneous Neumann boundary conditions.

$$\frac{\partial C}{\partial x}(0,t) = \frac{\partial C}{\partial x}(a,t) = 0 \qquad \text{(A-7)}$$

Initially the two polymer layers are unmixed. Hence, our initial profile can be described by step profile.

$$C(x,0) = C_0[1 - \mathcal{H}(x - b)] \qquad a > b > 0 \qquad \text{(A-8)}$$

where C_0 is the concentration of the diffusant polymer on the ATR element and $\mathcal{H}$ is the Heaviside function. Solution of the initial/boundary-value problem defined in eqs A-6–A-8 provides the following expression for the time-dependent concentration profiles.

$$\frac{C(x,t)}{C_0} = \frac{b}{a} + \frac{2}{\pi}\sum_{n=1}^{\infty}\frac{\sin\left(n\pi\frac{b}{a}\right)}{n}\cos\left(n\pi\frac{x}{a}\right)\exp\left(-n^2\pi^2\frac{Dt}{a^2}\right) \qquad \text{(A-9)}$$

The ATR technique does not measure directly concentration profiles, but an absorbance, A_t, which is proportional to the instantaneous mass which is spatially weighted over the detection volume determined by the ATR

penetration depth.

$$A_t = \int_0^a \alpha \exp(-2x/\lambda) C(x,t)\, S\, dx \qquad \text{(A-10)}$$

where α is the oscillator strength, λ is the characteristic penetration depth for the evanescent FTIR beam's electric field, and S is the cross-sectional area. The experimental measurements of absorbance can be normalized between the initial absorbance value and that at infinite time. Using eqs A-9 and A-10, we obtain eq 4. It is important to note that the diffusion coefficient is the only adjustable parameter used to fit this model to the experimental sorption data.

The second model considers the situation where the matrix is swellable only to a finite degree by the diffusant. Hence, a moving boundary exists where the diffusant concentration attains its solubility, K_s. There is no diffusive penetration of the matrix polymer into the diffusant thin film. Volume of mixing is not considered. The initial concentration profile is still described by eq A-8; however, moving boundary conditions exist as the matrix settles into the thin film of diffusant. Initially the time-dependent boundary position, $b_t(t)$, is at the thin film thickness b.

$$b_t(0) = b \qquad \text{(A-11)}$$

At this front the concentration is specified at its solubility limit.

$$C(b_t,t) = C_0 K_s \qquad \text{(A-12)}$$

The position of the moving front is determined by a continuity balance of the diffusant across the front.

$$\frac{C_0}{K_s}\frac{db_t}{dt} = D\frac{\partial C}{\partial x}(b_t,t) \qquad \text{(A-13)}$$

There is no material flux across the opposite side of the matrix which is located at position $L_t = a - b + b_t$.

$$\frac{\partial C}{\partial x}(L_t,t) = 0 \qquad \text{(A-14)}$$

The diffusant sorption within the matrix is governed by Fick's law.

$$\frac{\partial C}{\partial t} = D\frac{\partial^2 C}{\partial x^2} \qquad x \in [b_t,L_t],\ t \in [0,\infty) \qquad \text{(A-15)}$$

This model is implemented using analytical solutions for the diffusant concentration profiles within the matrix and the moving boundary position. The absorbance is integrated numerically using eq A-10. The boundary conditions would change to those in eq A-7 when the matrix contacts the ATR element, i.e., $b_t(t) = 0$, and the computer algorithm implements this situation. However, this situation does not occur during the time scale of our measurements of PEI sorption in PEKK. It is important to note that both the diffusion coefficient and solubility are adjustable parameters used to fit this model to the experimental sorption data.

References and Notes

(1) Li, Y.; Stein, M.; Jungnickel, B. J. *Colloid Polym. Sci.* **1991**, *269*, 772.
(2) Defieuw, G.; Groeninckx, G.; Reynaers, H. *Polym. Commun.* **1989**, *30*, 267.
(3) Cheng, S. Z. D.; Barley, J. S.; von Meerwall, E. D. *J. Polym. Sci., Polym. Phys. Ed.* **1991**, *29*, 515.
(4) John, E.; Ree, T. *J. Polym. Sci., Polym. Chem. Ed.* **1990**, *28*, 385.
(5) Roland, C. M. *Macromolecules* **1987**, *20*, 2557.
(6) Billingham, N. C.; Calvert, P. D.; Uzuner, A. *Polymer* **1990**, *31*, 258.
(7) Ryan, T. G.; Calvert, P. D. *Polymer* **1982**, *23*, 877.
(8) Tead, S. F.; Kramer, E. J.; Russell, T. P.; Volksen, W. *Polymer* **1992**, *33*, 3382.
(9) Filippov, A. V.; Smirnov, V. S.; Doroginitskii, M. M.; Gimatdinov, R. S. *Vysokomol. Soedin., Ser. B.* **1989**, *31*, 72; English transl. *Int. Polym. Sci. Technol.* **1989**, *16*, transl. serial no. 11045.
(10) Meakin, P. J.; Cogswell, F. N.; Halbritter, A. J.; Smiley, A. J.; Staniland, P. A. *Compos. Manuf.* **1991**, *2*, 86.
(11) Zwanzig, R. *J. Phys. Chem.* **1992**, *96*, 3926.
(12) Teraoka, I.; Langley, K. H.; Karasz, F. E. *Macromolecules* **1992**, *25*, 6106.
(13) Sahimi, M.; Hughes, B. D.; Scriven, B. D.; Davis, H. T. *J. Chem. Phys.* **1983**, *78*, 6849.
(14) Sahimi, M. *J. Chem. Phys.* **1992**, *96*, 4718.
(15) Shah, N.; Ottino, J. M. *Chem. Eng. Sci.* **1986**, *41*, 283.
(16) Shah, N.; Sax, J. E.; Ottino, J. M. *Polymer* **1985**, *26*, 1239.
(17) Kremer, K.; Binder, K. *J. Chem. Phys.* **1984**, *81*, 6381.
(18) Baumgartner, A.; Muthukumar, M. *J. Chem. Phys.* **1987**, *81*, 3082. Muthukumar, M.; Baumgartner, A. *Macromolecules* **1989**, *22*, 1937, 1941. Baumgartner, A. In *Springer Series in Chemical Physics*; Tanaka, F., Doi, M., Ohta, T., Eds.; Springer-Verlag: Berlin, 1989; Vol. 51.
(19) Honeycutt, J. D.; Thirumalai, D. *J. Chem. Phys.* **1989**, *90*, 4542.
(20) Chang, I. Y. *SAMPE Quart.* **1988**, *19*, 29.
(21) Sauer, B. B.; Avakian, P.; Starkweather, H. W., Jr.; Hsiao, B. S. *Macromolecules* **1990**, *23*, 5119.
(22) Hsiao, B.; Chang, I. Y.; Sauer, B. B. *Polymer* **1991**, *32*, 2799.
(23) Gardner, K. H.; Hsiao, B. S.; Matheson, R. R.; Wood, B. A. *Polymer* **1992**, *33*, 2483.
(24) Hsiao, B. S.; Sauer, B. B. *J. Polym. Sci., Polym. Phys. Ed.*, in press.
(25) Van Alsten, J. G.; Lustig, S. R. *Macromolecules* **1992**, *25*, 5069.
(26) Koberstein, J. T.; Morra, B.; Stein, R. S. *J. Appl. Crystallogr.* **1980**, *13*, 34.
(27) Vonk, C. G.; Kortleve, G. *Kolloid Z.* **1967**, *220*, 19.
(28) Kortleve, G.; Vonk, C. G. *Kolloid Z.* **1968**, *225*, 124.
(29) Strobl, G. R.; Schneider, M. *J. Polym. Sci., Polym. Phys. Ed.* **1980**, *18*, 1340.
(30) Santa Cruz, C.; Stribeck, N.; Zachmann, H. G.; Balta Calleja, F. J. *Macromolecules* **1991**, *24*, 5980.
(31) Harrick, N. J. *Internal Reflection Spectroscopy*; Wiley: New York, 1967.
(32) Salzberg, C. D. *J. Opt. Soc. Am.* **1957**, *47*, 244.
(33) Tirrell, M. *Rubber Chem. Technol.* **1984**, *57*, 523.
(34) Lovinger, A. J.; Davis, D. D. *J. Appl. Phys.* **1985**, *58*, 2843.
(35) Olabisi, O.; Robeson, L. M.; Shaw, M. T. *Polymer–Polymer Miscibility*; Academic Press: New York, 1979.
(36) Van Alsten, J. G.; Lustig, S. R.; Hsiao, B. S. *Bull. Am. Phys. Soc.* **1983**, *38* (1), 657.
(37) Michaels, A. S.; Paker, R. B. *J. Polym. Sci.* **1959**, *41*, 53. Michaels, A. S.; Bixler, H. J. *J. Polym. Sci.* **1961**, *50*, 391.
(38) Sax, J.; Ottino, J. M. *Polym. Eng. Sci.* **1983**, *23*, 165.
(39) Ottino, J. M.; Shah, N. *Polym. Eng. Sci.* **1984**, *24*, 153.
(40) Stauffer, D. *Introduction to Percolation Theory*; Taylor and Francis: London, 1985.